Multi-temporal RADARSAT-1 and ERS Backscattering Signatur es of Coastal Wetlands in Southeaster n Louisiana

Oh-ig Kwoun and Zhong Lu

Abstract

Using multi-temporal European Remote-sensing Satellites (ERS-1/-2) and Canadian Radar Satellite (RADARSAT-1) synthetic aperture radar (SAR) data over the Louisiana coastal zone, we characterize seasonal variations of radar backscattering according to vegetation type. Our main findings are as follows. First, ERS-1/-2 and RADARSAT-1 require careful radiometric calibration to perform multi-temporal backscattering analysis for wetland mapping. We use SAR backscattering signals from cities for the relative calibration. Second, using seasonally averaged backscattering coefficients from ERS-1/-2 and RADARSAT-1, we can differentiate most forests (bottomland and swamp forests) and marshes (freshwater, intermediate, brackish, and saline marshes) in coastal wetlands. The student t-test results support the usefulness of season-averaged backscatter data for classification. Third, combining SAR backscattering coefficients and an optical-sensor-based normalized difference vegetation index can provide further insight into vegetation type and enhance the separation between forests and marshes. Our study demonstrates that SAR can provide necessary information to characterize coastal wetlands and monitor their changes.

Introduction

Coastal wetlands constitute important ecosystems in terms of flood control, water and nutrient storage, habitat for fish and wildlife reproduction and nursery activities, and overall support of the food chain (Karszenbaum *et al.*, 2000). The integrity of such wetlands has significant ecologic and economic implications. Louisiana has one of the largest expanses of coastal wetlands in the conterminous United States, and its coastal wetlands contain an extraordinary diversity of habitats. The unique habitats of upland areas and the Gulf of Mexico, complex hydrological connections, and migratory routes of birds, fish, and other species place the coastal wetlands of Louisiana among the nation's most productive and important natural assets (USACOE, 2004).

However, the balance of Louisiana's coastal systems has been upset by a combination of natural processes and human activities. Massive coastal erosion probably started around 1890, and more than one million acres or about 20 percent of the coastal lowlands (mostly wetlands) have eroded in the past 100 years (LCWCRTF/WCRA, 1998). For example, the loss rate for Louisiana's coastal wetlands was as high as 25,200 and 15,300 acres per year in 1970s and 1990s, respectively (Barras *et al.*, 2003). Massive environmental changes have significant impacts on the coastal ecosystem of Louisiana, including effects from frequent natural disasters such as the Hurricane Katrina in 2005. Therefore, an effective method of mapping and monitoring coastal wetlands is essential to understanding the status and influence of environmental changes and human activities on wetlands.

Optical satellite images such as those from Landsat Thematic Mapper (TM) and Enhanced Thematic Mapper Plus (ETM+) have been used to map coastal wetlands (Homer *et al.*, 2004; Loveland and Shaw, 1996). For example, National Land-cover Data 1992 was created from Landsat TM data; the producer's accuracy for wetlands over the southeastern region of the United States was assessed at 46 ~ 77 percent (Stehman *et al.*, 2003). A unique characteristic of synthetic aperture radar (SAR) in monitoring wetlands over cloud-prone subtropical regions is the all-weather and day-and-night imaging capability. In addition, SAR can provide key descriptors for a wetland environment, such as ground vegetation structure, inundation, topographic features, and moisture content (Sadre *et al.*, 1995).

Waite and MacDonald (1971) first reported that flooded forests in "leaf off" conditions in Arkansas showed up as anomalously bright areas on K-band radar images. Since then, several studies have demonstrated that satellite SAR can map and monitor forested and non-forested wetlands occupying a range of coastal and inland settings (Ramsey III, 1998 and 1999; Ramsey III *et al.*, 2006). Many of those studies relied on the fact that when standing water is present beneath the vegetation canopies, the radar backscattering signal changes with water level changes, depending on vegetation type and structure. Therefore, they used SAR backscattering signals to monitor floods and dry conditions, temporal variations in the hydrological conditions of wetlands, including classification of wetland vegetation at various study sites (Baghdadi *et al.*, 2001; Bourgeau-Chavez *et al.*, 2001; Bourgeau-Chavez *et al.*, 2005; Costa, 2004; Costa *et al.*, 2002; Grings *et al.*, 2006; Hess and Melack, 1994; Hess

Oh-ig Kwoun is with Jet Propulsion Laboratory, California Institute of Technology, Pasadena, CA 91109, and formerly with SAIC at the U.S. Geological Survey, EROS Data Center, Sioux Falls, SD 57198 (kwoun@jpl.nasa.gov).

Zhong Lu is with the USGS EROS Center and Cascades Volcano Observatory, Vancouver, WA 98683 (lu@usgs.gov).

Photogrammetric Engineering & Remote Sensing
Vol. 75. No. 5, May 2009, pp. 607–617.

0099-1112/09/7505–0607/$3.00/0

et al., 1995; Horritt *et al.*, 2003; Karszenbaum *et al.*, 2000; Kasischke and Bourgeau-Chavez, 1997; Kiage *et al.*, 2005; Le Toan *et al.*, 1997; Lu *et al.*, 2005; Ramsey III, 1995; Simard *et al.*, 2002; Townsend, 2002). Previous studies using satellite SAR imagery over coastal Louisiana were focused on flood detection in wetland and urban areas with a limited number of scenes (Kiage *et al.*, 2005; Russell *et al.*, 2005).

The primary objective of our study is to derive robust indicators, which are based on multiple temporal SAR images from two different sensors, to differentiate vegetation types over coastal wetlands. We use SAR data acquired from two sensors during several consecutive years to assess the potential of C-band SAR imagery for characterizing and monitoring wetland vegetation in a coastal flood zone. The multitemporal SAR data from European Remote-sensing Satellites (ERS-1/-2) and Canadian Radar Satellite (RADARSAT-1) were acquired during both leaf-on and leaf-off seasons to allow the study of temporal variation of SAR backscattering. The multitemporal data sets also help us overcome temporary environmental effects to provide robust results. We first demonstrate the necessity of relative calibration of SAR backscattering signals prior to inferring the relationship between SAR returns and wetland types. We then investigate how radar backscattering signals from different vegetation classes vary with time and whether those vegetation classes have distinguishable radar backscattering signatures. Our goal is to infer the vegetation structure from calibrated SAR backscattering returns. Finally, we evaluate the relationship between radar backscattering coefficients and normalized difference vegetation indices derived from optical images to provide additional information to differentiate wetland classes.

Study Site

Coastal Louisiana is made up of two wetland-dominated ecosystems: the Deltaic Plain of the Mississippi River (eastern region) and the Chenier Plain (western region). Our study area covers the Barataria, Terrebonne, and Atchafalaya River Basins and the Teche/Vermilion Basin within the Deltaic Plain (Plate 1). We combine the land-cover classification map from the Louisiana Gap Analysis Program (GAP) (USGS-NWRC, 1998) and the land-cover map by Barras *et al.* (1994) as the base map for land-cover types. We focus on nine major land-cover types: bottomland forest, swamp forest, freshwater marsh, intermediate marsh, brackish marsh, saline marsh, open water, agriculture, and urban (Plate 1). A good description of different types of vegetation in the study area can be found at **http://la.water.usgs.gov/nawqa/ecology.htm** and **http://plants.ifas.ufl.edu/photocat.html**. Typical plants and salinity concentration, according to LCWCRTF/WCRA (1998) within each wetland class are listed in Table 1.

Agriculture and urban land-cover types are found in relatively high elevation areas along the well-established access roads (Plate 1). Sugarcane, soybean, and forage

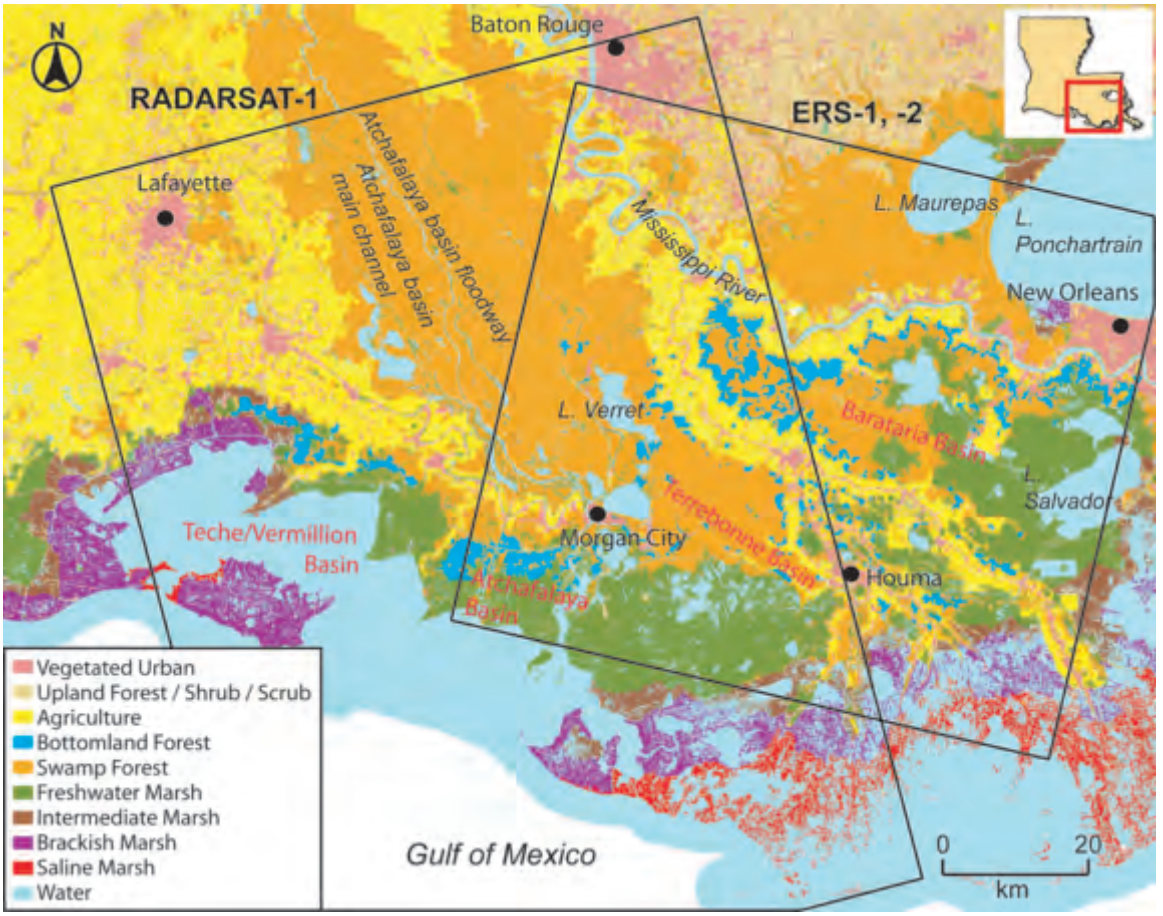

Plate 1. Modified GAP land-cover map of southeastern Louisiana. Polygons represent the coverage of ERS and RADARSAT-1 SAR images.

TABLE 1. VEGETATION CLASSES AND TYPICAL PLANTS OVER COASTAL SOUTHEASTERN LOUISIANA [1]

Vegetation Classes	Typical Plants	Salinity
Bottomland forests	American elm (*Ulmus americana*) Sweetgum (*Liquidambar styraciflua*) Sugarberry (*Celtis laevigata*) Swamp red maple (*Acer rubrum var. drummondii*)	N/A
Swamp forests	Bald cypress (*Taxodium distichum*) Water tupelo (*Nyssa aquatica*)	0 ~ 1 ppt[2]
Freshwater marshes	Maidencane (*Panicum hemitomon*) Spikerush (*Eleocharis* sp.) Bulltongue (*Sagittaria falcata*)	0 ~ 3 ppt
Intermediate marshes	Bulltongue (*Sagittaria falcata*) Saltmeadow cordgrass or wire grass (*Spartina patens*)	2 ~ 5 ppt
Brackish marshes	Saltmeadow cordgrass or wire grass (*Spartina patens*) Three-square bulrush (*Scirpus americana*)	4 ~ 15 ppt
Saline marshes	Smooth cordgrass or oyster grass (*Spartina alterniflora*) Saltgrass (*Distichlis spicata*)	12 ppt and higher

1. Modified from (LCWCRTF/WCRA, 1998)
2. Parts-per-thousand

constitute the primary agriculture classes (Chabreck, 1972; LCWCRTF/WCRA, 1998). Bottomland forests represent a transition between drier upland hardwood forest and very wet river floodplain and wetland forests (Plate 1). Bottomland forests are intermittently inundated (IFAS, 2006). Swamp forests are found in the lowest elevation areas and are inundated most of the time (IFAS, 2006). Swamp forest in Louisiana is mostly comprised of bald cypress and water tupelo, and the salinity of the flooded water ranges from 0 ~ 1 parts-per-thousand (ppt). The plants that live in swamp forests have adapted to tolerate high water levels.

The freshwater marsh community is comprised largely of floating marshes (Plate 1). Maidencane, spikerush, and bulltongue comprise the dominant species. Freshwater marshes have the greatest plant diversity and the highest soil organic matter content of any marsh type over the study area (Chabreck, 1972). However, plant diversity varies with location, and many areas of monotypic marshes can be found in the Louisiana coastal zone (E. Ramsey, personal communication, 2007). The salinity of freshwater marsh ranges 0 ~ 3 ppt (LCWCRTF/WCRA, 1998; Nelson *et al.*, 2002).

With a salinity level of 2 ~ 5 ppt, intermediate marshes represent a zone of mild salt content, which results in fewer plant species than freshwater marsh (Chabreck, 1972) (Plate 1). The intermediate marsh can be characterized as plant species common to freshwater marsh but with saltier versions of them toward the sea. Intermediate marsh is largely composed of bulltongue and saltmeadow cordgrass (LCWCRTF/WCRA, 1998). The latter, also called wire grass, is not found in freshwater marsh (Barras *et al.*, 2006).

Brackish marshes have salinity of 4 ~ 15 ppt and are irregularly flooded by tide (Plate 1); they are largely composed of wire grass and three-square bullrush. This marsh community can be described as marshes that are virtually all wire grass, i.e., clusters of three-foot-long grass-like leaves, with little variation in plant species (Barras *et al.*, 2006).

The saline marsh community has the largest saline concentration (12 ppt and higher) (LCWCRTF/WCRA, 1998) (Plate 1). With the least diversity of vegetation species, saline marsh is largely composed of smooth cordgrass, oyster grass, and saltgrass.

The hydrologic status of marsh areas is such that freshwater marshes occur in relatively low energy environments and may be subject to tidal changes, but not ebb and flow. They change slowly and have thick sequences of organic soils or floating grass root mats. Saline and brackish marshes are found in high energy areas and are subject to the ebb and flow of the tides (LCWCRTF/WCRA, 1998).

Data and Processing

SAR Data

In this study, ERS-1 (11 scenes) and ERS-2 (22 scenes) data between 1992 and 1998, and RADARSAT-1 (19 scenes) data from 2002 to 2004 are used for backscattering analysis (Table 2). ERS data were acquired during descending

TABLE 2. SAR SENSOR CHARACTERISTICS: SENSOR, BEAM MODE, ORBIT DIRECTION, INCIDENCE ANGLE

Satellite	Image Acquisition Dates (year: mm/dd)
ERS-1 (C-VV) Orbit pass: Descending Incidence angle at scene center: 23.3°	1992: 06/11, 07/16, 08/20, 09/24, 10/29 1993: 01/07, 04/22, 09/09 1995: 11/11 1996: 01/20, 05/04 (11 scenes)
ERS-2 (C-VV) Orbit pass: Descending Polarization: C-VV Incidence angle: 23.3°	1995: 11/12, 12/17 1996: 01/21, 05/05, 06/09, 07/14, 08/18, 09/22, 10/27, 12/01 1997: 01/05, 03/16, 05/25, 09/07, 10/12, 11/16 1998: 01/25, 03/01, 04/05, 07/19, 08/23, 09/27 (22 scenes)
RADARSAT-1 (C-HH) Orbit pass: Ascending Incidence angle: 27.7°	2002: 05/03, 05/27, 06/20, 07/14, 08/07, 08/31, 11/11 2003: 02/15, 05/22, 06/15, 07/09, 08/02, 10/12, 12/23 2004: 02/09, 03/28, 04/21, 07/02, 09/12 (19 scenes)

passes and RADARSAT-1 data during ascending passes. The spatial coverage of both ERS and RADARSAT-1 scenes is shown in Plate 1.

As precipitation can affect the moisture content of vegetation and soil that control the SAR backscattering returns (Lu and Meyer, 2002), we checked the precipitation information at the SAR image acquisition dates. During the RADARSAT-1 image acquisitions (2002 ~ 2004), the precipitation records at four weather stations over our study region were available. During 1992 through 1999 when ERS-1/-2 images were acquired, only one weather station maintained the precipitation information. Our regression analyses between the amount of precipitation and the SAR backscatter signal did not reveal any meaningful correlation. Conservatively, however, we excluded all scenes when the precipitation was more than one inch/day.

SAR raw data are processed into single-look complex (SLC) images with antenna pattern compensation. The intensity of the SLC image in converted into the backscattering coefficient, σ° according to Wegmüller and Werner (2003). The topography of Southern Louisiana is almost flat; therefore, additional adjustment of σ° for local terrain slope effect is not necessary.

ERS-1 and ERS-2 SLC images are co-registered to a common reference image using a two-dimensional *sinc* function (Wegmüller and Werner, 2003). ERS-2 orbit 7452, acquired on 22 September 1996 is the reference image used to minimize baseline diversity. The co-registered SLC images are multi-looked using a 2 × 10 window to represent a ground-projected pixel size of about 40 m × 40 m. The same procedure is used to process RADARSAT-1 data. All SLC images are co-registered to a common reference image (orbit 40409, acquired on 02 August 2003); the co-registered data are multi-looked with a 3 × 10 window to represent a ground-projected pixel size of approximately 53 m × 53 m. Speckle noise in the images is suppressed using the Frost adaptive despeckle filter (Frost *et al.*, 1982) with a 3 × 3 window size on the co-registered and multi-looked images. Finally, SAR images are geo-referenced and co-registered with the modified GAP land-cover map.

SAR Data Calibration

We have selected many data samples across the study area to examine seasonal variation of σ° for different vegetation types. Locations of data samples are shown in Figure 1. For each of the nine land-cover classes, between three and nine locations distributed across the study area have been chosen for backscattering analysis. The 2004 Digital Orthophoto Quarter Quadrangle (DOQQ) imagery for Louisiana (USGS-NWRC, 2005) is used to verify the land-cover type over the sampling sites. The size of sampling boxes varies between 3 × 3 pixels and 41 × 41 pixels, so that each box may cover only a single land-cover type. The DOQQ imagery is also used to ensure the homogeneity of samples at each site.

The results of average σ° for each class are shown in Figure 2. The overall difference in the average σ° between Figure 2a and 2b is due to differences in sensors and environmental changes. The σ°_{ERS} shows a generally downward degrading trend (Figure 2a). This long-term declination is present for all land-cover classes, suggesting ERS-2 has a temporal decrease of antenna power. Meadows *et al.* (2004) reported that, since the launch in 1995 until the end of 2000, ERS-2 antenna transmission degraded at the rate of 0.66 dB per year. Therefore, we compensated for this long-term declination of σ° before further analysis.

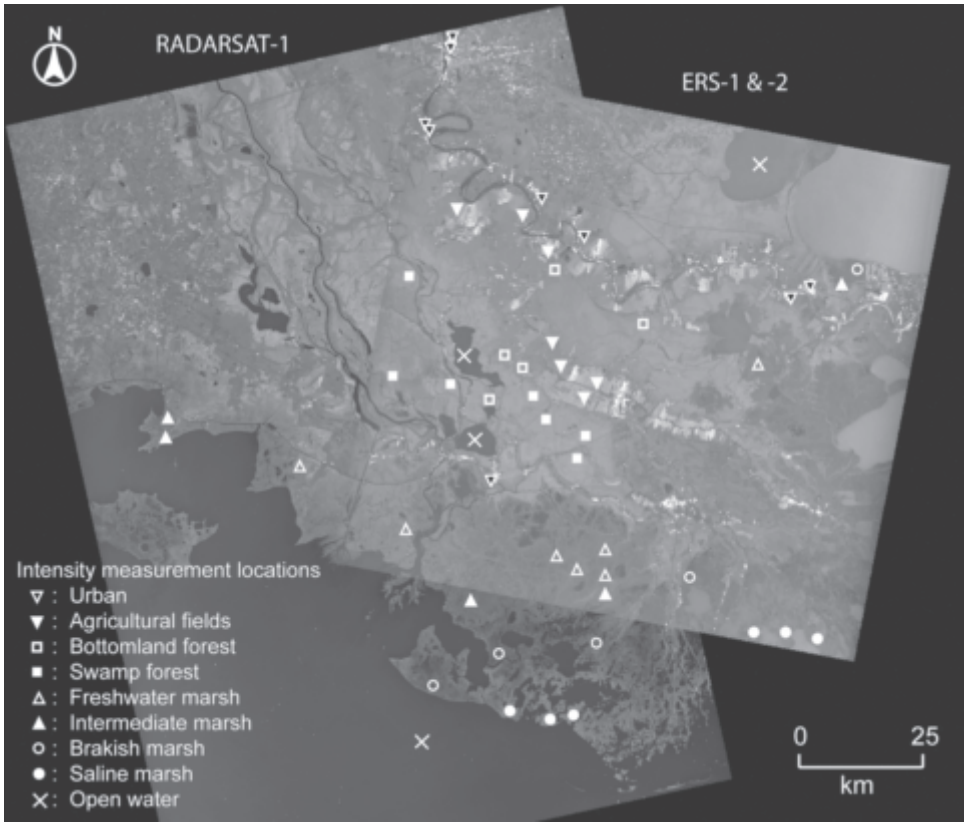

Figure 1. Averaged SAR intensity image mosaic with locations of data sample sites.

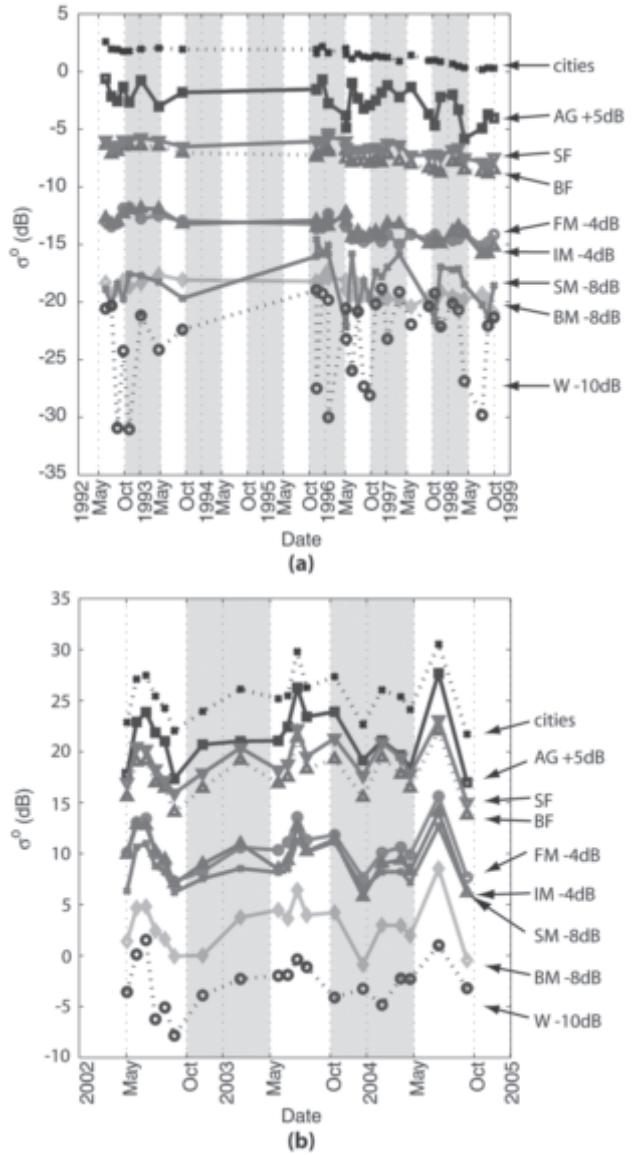

Figure 2. Temporal variations of radar backscattering coefficient from (a) ERS-1/-2, and (b) RADARSAT-1. (Note: AG is agricultural field, SF is swamp forest, BF is bottomland forest, FM is freshwater marsh, IM is intermediate marsh, BM is brackish marsh, SM is saline marsh, and W is open water). A color version of this figure is available at the ASPRS website: **www.asprs.org.**

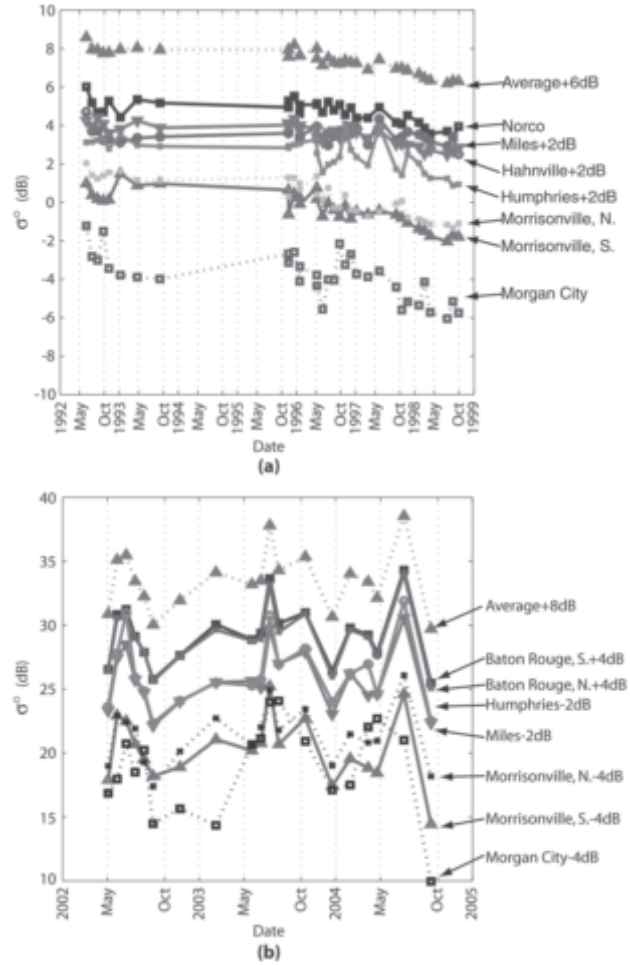

Figure 3. Temporal variations of radar backscattering coefficient over cities from (a) ERS-1/-2, and(b) RADARSAT-1. A color version of this figure is available at the ASPRS website: **www.asprs.org**.

Unlike ERS, $\sigma^{\circ}_{RADARSAT}$ exhibits strong temporal variation for all land-cover types (Figure 2b). We find that $\sigma^{\circ}_{RADARSAT}$ over water mimics the variation of σ° over other land classes. This strongly suggests that the temporal variation in RADARSAT-1 is caused not only by changes in environmental conditions but also by some systematic changes that we do not understand. They need to be removed prior to any further analysis of σ°.

Extensive homogeneous surfaces with known backscattering characteristics, such as Amazon forests or carefully designed corner reflectors, are ideal for radiometric calibration, but no such locations exist in our study site. However, many artificial structures and objects in cities, such as buildings, roads, and industrial facilities may be considered corner-reflector complex and behave like permanent scatterers whose backscattering characteristics do not change with time despite environmental variation (Ferretti *et al.*, 2001). Under ideal conditions, backscattering coefficients from urban areas should remain almost constant over time, and therefore they can be used as an alternative to calibrate time-varying radar backscattering characteristics.

Most of the cities in coastal Louisiana are mixed with vegetation, implying that the radar backscattering from these areas can be affected by vegetation responses. Figure 3 shows temporal variation of the σ° mean from six cities for ERS data and five cities for RADARSAT-1 data. The variation of σ° from Morgan City is quite different from the rest of the cities. Inspecting high-resolution DOQQ images over these cities suggests that Morgan City has the largest percentage of vegetation coverage. Therefore, we interpret the low σ°_{ERS} and $\sigma^{\circ}_{RADARSAT}$ of Morgan City as due to the effect of urban vegetation on radar backscattering return. In addition, Humphries shows anomalous backscattering changes in 1996 and 1997. Therefore, for each SAR image, σ°s from the remaining cities are averaged to obtain the mean backscattering coefficient of urban areas (Figure 3). The large difference between Norco and the rest of cities in ERS data (Figure 3a) is probably

because fully developed industrial facilities and urban infrastructure in Norco are aligned more favorably for double-bounce returns than other cities. However, variation of σ° over Norco follows a similar trend of σ° for other cities.

Because temporal variation of backscattering coefficients over urban areas is very similar, we assume that the cause of the systematic variation affects not only the city areas but also the whole study region in the same manner. Therefore, relative calibration with σ° over urban areas compensates these systematic patterns of σ° for the rest of the land-cover types. Accordingly, for each SAR scene, the averaged σ° value of urban areas from the corresponding image is used as the reference and subtracted from σ° values of other land-cover classes in that individual image. We then use the "calibrated" σ° to study backscattering characteristics of different land-covers and their seasonal changes. Plate 2a and 2b show seasonally averaged σ° of each land-cover type for leaf-on and leaf-off seasons after relative calibration.

Analysis and Discussion

Possible Radar Backscattering Mechanisms over the Study Site

Over vegetated terrain, the incoming radar wave interacts with elements of the vegetation as well as the ground surface. Part of the energy is attenuated, and the rest is scattered back to the antenna. The amount of radar energy returned to the antenna (backscattering signal) depends on the size, density, shape, and dielectric constants of the target, as well as SAR system characteristics, such as incidence angle, polarization, and wavelength (Kiage *et al.*, 2005; Ulaby and Dobson, 1989). The dielectric constant, or permittivity, describes how a surface attenuates or transmits the incoming radar wave. Live vegetation with high water content has a higher dielectric constant than drier leaves. This implies that a stronger backscattering signal is expected from a wet surface than a drier surface. The transmission of the radar signal through the canopy is also directly related to the characteristics of the radar (e.g., long wavelength radar such as L-band Advanced Land Observing Satellite (ALOS) tends to penetrate through the canopy better than short wavelength radar such as C-band ERS or RADARSAT) as well as the canopy structures. Therefore, comparing the calibrated σ° values from various vegetation canopies in diverse environments can provide insight into the canopy structure.

Over the study site, radar signal backscattering mechanisms can be simplified into four major categories: surface scattering, volume scattering, double-bounced scattering, and specular scattering. Figure 4 illustrates how different structural layers of vegetation affect the way a radar signal returns. Forested wetlands often develop into distinct layers, such as an overstory of dominant tree species, an understory of companion trees and shrubs, and a ground layer of herbaceous plants (IFAS, 2006). Therefore, over a dense forest, the illuminating radar signal scatters from the canopy surface, and a fraction of the energy is returned to the antenna. This phenomenon is called surface scattering. The remaining radar wave penetrates into and interacts with the vegetation volume, and a portion of the energy is returned to the antenna. This results in volume scattering. Volume scattering can also dominate moderately dense forest with dense understory (Figure 4a). In moderately dense forested canopy, some microwave energy penetrates through the overstory and interacts with tree trunks and the ground layer. If the ground is flooded, a large portion of the microwave energy is forward scattered off the tree trunks,

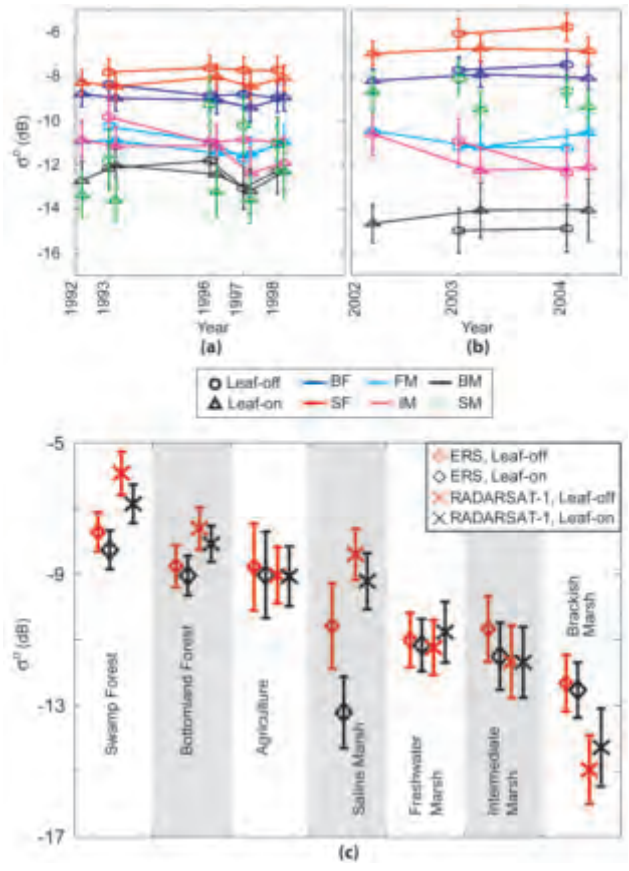

Plate 2. Seasonally averaged (a) ERS-1/-2, and (b) RADARSAT-1 radar backscattering coefficients (σ°) of each land-cover type during leaf-on and leaf-off seasons. Relative calibration is done with the averaged σ° of urban areas; (c) Multi-year seasonally averaged σ° values and their standard deviations of each land-cover type.

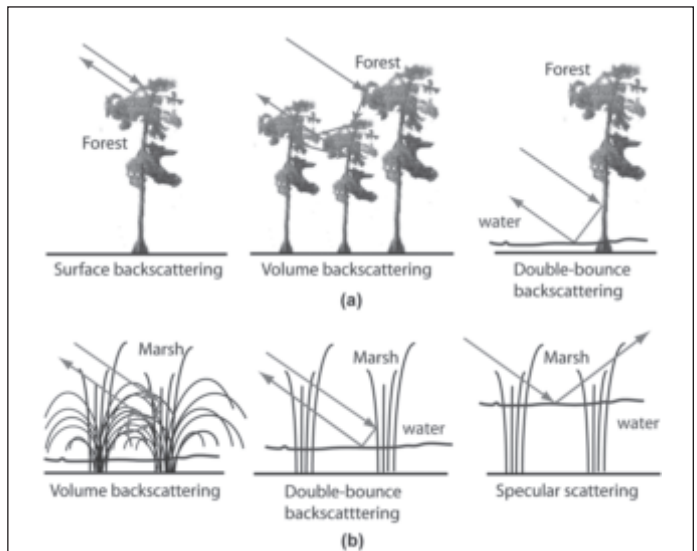

Figure 4. Schematic diagrams showing interactions between the radar signal and (a) forests, and (b) marshes.

bounced off the smooth water surface, and then back to the radar antenna. This phenomenon is called "double-bounced" scattering (Figure 4a). Because more microwave energy is scattered back to the antenna than other types of backscattering, the detected SAR image should have enhanced intensity compared to other types of vegetation canopy where volumetric scattering dominates.

Over herbaceous canopies, SAR can often penetrate through the vegetation to reach the ground surface depending on the vegetation density. If the soil is dry, multiple scatterings between vegetation and the ground surface can attenuate the incoming radar signal, and the energy back to the radar is reduced. If the soil is wet, the higher dielectric constant of the soil reduces the transmission of the radar wave and enhances the backscattering return. If the ground is flooded, and the above-water stems are large enough and properly oriented to allow double-bounce between the water surface and stems, the backscattering signal is significantly enhanced (i.e., "double-bounced" scattering) (Figure 4b). If the ground is completely flooded, and vegetation canopy is almost submerged, there is little chance for the radar signal to interact between canopy stems and water surface. Instead, most of the radar energy is scattered away from the antenna (i.e., "specular" scattering) (Figure 4b). As a result, little energy is bounced back to the radar. Floating aquatic vegetation and short vegetation in flooded area may exhibit similar backscattering returns and therefore can not be distinguished from SAR backscattering values. In general, the overall bulk density of these vegetation classes may determine the total amount of SAR signal that can be backscattered to the senor.

Radar Backscattering over Different Land-cover Classes

For the purpose of analyzing seasonal backscattering changes, we split a typical year into two seasons. As previously summarized, we use the normalized difference vegetation index (NDVI) to identify the peaks of "green-up," which occur around early May and early October (Figure 5a and 5b). For convenience, we refer to the summer, between May and October, as the "leaf-on" season, and the rest of the year as the "leaf-off" season. However, our definition of "leaf-off" does not necessarily mean that the vegetation has no leaf, as one may expect of deciduous trees in high latitude regions. Over our study area, some marsh types exhibit little, if any, seasonal variation (e.g., black needlerush); others change green biomass percentage; and others completely overturn (E. Ramsey, personal communication, 2007). We then use the "calibrated" σ° and average it by season to study backscattering characteristics of different land-covers and their seasonal changes (Plate 2).

The agricultural fields over the study area do not follow the natural cycle of vegetation. Multiple harvests and plowing drastically change surface roughness and moisture conditions, which significantly alter radar-backscattering values. Therefore, we exclude agriculture from further analysis.

The σ° values of swamp forests are the highest among all of the vegetation classes under investigation (Plate 2a and 2b). This suggests that the density of trees is moderate or sparse enough and the density of understory, if any, is low enough to allow penetration of the C-band SAR signal to interact with the water surface for double-bounce backscattering, which is consistent with the report by Lu *et al.* (2005) based on interferometric analyses. Plate 2a and 2b show that the mean σ° values of swamp forests from ERS and RADARSAT-1 are about 0.54 dB and 0.93 dB higher during leaf-off seasons than leaf-on seasons, respectively. Seasonal backscatter changes over swamp forests are consistently larger than those of bottomland forests. This is probably because during leaf-on seasons, radar attenuation at the

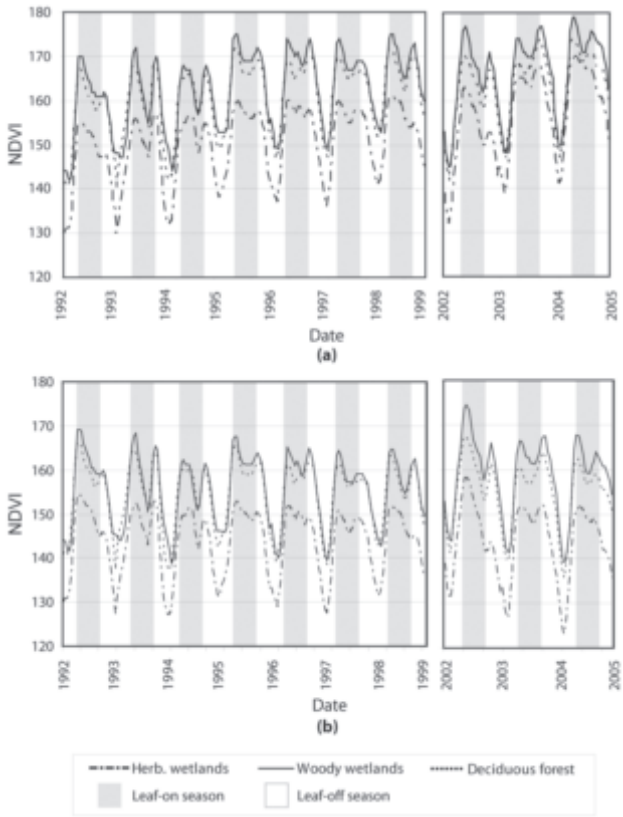

Figure 5. (a) NDVI values before adjusting the long-term trends for 1992 ~ 1998 and 2002 ~ 2004, and (b) NDVI values adjusted for long-term trends.

overstory is increased and double-bounced backscattering is reduced, which results in decreases in both σ° values and interferometric coherence (Lu *et al.*, 2005). We also observe that the $\sigma^\circ_{\text{RADARSAT}}$ during leaf-on seasons is about 0.86 dB higher than $\sigma^\circ_{\text{ERS}}$ during leaf-off season. This is consistent with a report by Freeman and Durden (1998). Using C-band AIRSAR data, they demonstrated that the mean σ° of HH-polarization (e.g., RADARSAT-1) was stronger than that of VV-polarization (e.g., ERS) over tropical forested wetlands, primarily due to double-bounced backscattering.

The bottomland forest has the second highest mean σ° values, ranging from $-9.4 \sim -8.4$ dB for ERS and $-8.2 \sim -7.5$ dB for RADARSAT-1 (Plate 2a and 2b). The averaged σ° of bottomland forests is consistently lower than that of swamp forests by 0.52 ~ 1.26 dB for ERS and 0.75 ~ 1.70 dB for RADARSAT-1, indicating weaker radar signal return from bottomland forest than swamp forest. We attribute this to the decreased double-bounced backscattering due to dense understory canopy, which is abundant in bottomland forests. Similar to the swamp forests, the averaged $\sigma^\circ_{\text{LEAF\_OFF}}$ is slightly higher than the averaged $\sigma^\circ_{\text{LEAF\_ON}}$; however, the difference is much smaller over bottomland forests than swamp forests. From the perspective of land-cover classification, comparison of σ° between bottomland and swamp forests indicates that averaged intensity of RADARSAT-1 data during any single year contains sufficient information to differentiate the two classes (Plate 2b and 2c).

Freshwater and intermediate marshes show relatively similar σ° for both ERS and RADARSAT-1. For freshwater marsh, the averaged $\sigma^\circ_{\text{ERS}}$ ranges between -11.0 ± 0.8 dB

and -11.2 ± 0.8 dB for leaf-off and leaf-on seasons, respectively, and $\sigma^{\circ}_{\text{RADARSAT}}$ ranges between -11.2 ± 0.8 dB and -10.8 ± 0.9 dB, respectively. For intermediate marsh, the averaged $\sigma^{\circ}_{\text{ERS}}$ ranges between -10.7 ± 1.0 dB and -11.5 ± 1.0 dB for leaf-off and leaf-on seasons, respectively, and $\sigma^{\circ}_{\text{RADARSAT}}$ ranges between -11.7 ± 1.1 dB and -11.7 ± 1.1 dB, respectively (Plate 2c).

The seasonal average values of $\sigma^{\circ}_{\text{ERS}}$ and $\sigma^{\circ}_{\text{RADARSAT}}$ of freshwater marshes do not show any distinctive trends (Plate 2a and 2b). As for intermediate marshes, the mean values of $\sigma^{\circ}_{\text{ERS}}$ during leaf-off season are about a $0.9 \sim 1.5$ dB higher than during leaf-on season, except for 1996; however, the averaged $\sigma^{\circ}_{\text{RADARSAT}}$ values do not show any consistent trends.

From the perspective of land-cover classification, Plate 2 indicates that freshwater marshes and intermediate marshes may not be easily distinguishable based on SAR backscattering signals. Even the comparison of averaged coherence between freshwater and intermediate marshes does not show a substantial difference (Lu and Kwoun, 2008). It should also be noted that, although fresh and intermediate marshes are outside the direct inundation of most tides, they could be flooded for extended time periods. In our analysis, those conditions are not included.

The seasonally averaged $\sigma^{\circ}_{\text{ERS}}$ of brackish marshes ranges from $-13.2 \sim -11.8$ dB, and $\sigma^{\circ}_{\text{RADARSAT}}$ ranges from $-15.0 \sim -14.1$ dB (Plate 2). The drastic difference between ERS and RADARSAT is probably because we could not co-locate sampling sites for the two sensors due to a limitation in the image coverage (Plate 1 and Figure 1). This dislocation could result in dramatic differences in canopy type and structure and hydrologic regime. The σ° value for brackish marsh is the lowest among all vegetation types in the study. The averaged $\sigma^{\circ}_{\text{RADARSAT}}$ during leaf-on seasons is about $0.8 \sim 0.9$ dB higher than leaf-off seasons, while $\sigma^{\circ}_{\text{ERS}}$ does not show any significant difference (Plate 2). From the perspective of land-cover classification, Plate 2 indicates that single-year SAR data, particularly RADARSAT-1, would be sufficient to distinguish brackish marshes from other vegetation communities.

In the case of saline marshes, we could not co-locate the sampling sites for RADARSAT and ERS data as in the case of brackish marshes (Plate 1 and Figure 1). The seasonally averaged $\sigma^{\circ}_{\text{ERS}}$ is in the range of $-13.6 \sim -9.3$ dB, and the $\sigma^{\circ}_{\text{RADARSAT}}$ is about $-9.5 \sim -8.1$ dB (Plate 2). The mean $\sigma^{\circ}_{\text{ERS\_LEAF\_ON}}$ of saline marshes is comparable to that of brackish marshes, and the mean $\sigma^{\circ}_{\text{ERS\_LEAF\_OFF}}$ shows considerably dynamic inter-seasonal change and is in the range of freshwater and intermediate marshes (Plate 2c). The averaged $\sigma^{\circ}_{\text{RADARSAT}}$ is comparable to that of bottomland forests (Plate 2c). Both ERS and RADARSAT data show that the averaged $\sigma^{\circ}_{\text{LEAF\_OFF}}$ is higher than the averaged $\sigma^{\circ}_{\text{LEAF\_ON}}$, as is the case with forests. The saline marsh community is inundated daily with salt water tides and is subjected to the ebb and flow of the tides (LCWCRTF/WCRA, 1998). Therefore, it provides a favorable condition for double-bounced scattering between stems and the water surface underneath. From the image classification perspective, RADARSAT data may be sufficient to distinguish saline marshes from other marsh classes. The mean value of $\sigma^{\circ}_{\text{ERS\_LEAF\_ON}}$ of saline marshes is so distinct that some level of ambiguity in $\sigma^{\circ}_{\text{RADARSAT}}$ between bottomland forests and saline marshes can be resolved. In addition, the proximity to salt water may be another indicator that separates these two communities.

The student *t*-test (e.g., Davis 1985) is carried out to quantify the separability among different vegetation classes based on the averaged SAR backscattering coefficients. First, from the means, standard deviations, and sample numbers of two vegetation classes, the *t* score and the degree of freedom are calculated. Then, the *t*-criterion is selected based on the confidence level of 95 percent. Finally, each vegetation type is comprehensively paired with each of the other vegetation classes to test the statistical separability of the averaged backscatter values shown in Plate 2. The student *t*-test results in *t*-scores larger than their corresponding *t*-criteria at the 95 percent confidence level in most of cases, implying that multi-temporal, seasonally averaged SAR backscatter coefficients can be used to separate the two corresponding vegetation classes at a confidence level of 95 percent or higher. However, in some cases, the *t*-test results suggest some of the vegetation types can not be distinguished at the 95 percent confidence level. Table 3 lists all cases where *t*-scores are equal to or less than the *t*-criteria at the 95 percent confidence level. In these cases (Table 3), the SAR backscattering values can not be used to distinguish the corresponding vegetation classes at the 95 percent confidence level. Between agriculture and bottomland forests, for example, the student *t*- test indicates the *t*-scores of 0.13 and 0.20 for ERS backscattering coefficients during both leaf-off and leaf-on seasons, respectively. These *t*-scores are far smaller than the corresponding *t*-criteria (1.98), meaning that the ERS backscattering data can not be used to differentiate between the two vegetation classes. Similarly, for the freshwater and intermediate marshes, the *t*-score is about 1.28 for leaf-on ERS backscatter data while the corresponding *t*-criterion is 2.10; this implies that leaf-on ERS data are not useful to differentiate between the freshwater and intermediate marshes. However, the leaf-on RADARSAT data are able to differentiate between the two vegetations at the 95 percent confidence level as the *t*-score (4.48) is much larger than the corresponding *t*-criterion (2.01).

In summary, to classify wetland classes over the study area, the seasonal σ° values averaged over multiple years can be used to distinguish among bottomland forests, swamp forests, saline marshes, brackish marshes, and freshwater and intermediate marshes. Forests versus marshes can be identified because the $\sigma^{\circ}_{\text{ERS\_LEAF\_ON}}$ of marshes is significantly lower than that of forests. Swamp forests are marked with the highest σ° values from both ERS and RADARSAT-1.

TABLE 3. STUDENT T-TEST SCORES AND T-CRITERIA AT THE 95 PERCENT CONFIDENCE LEVEL FOR CASES WHERE SAR BACKSCATTERING COEFFICIENTS CANNOT BE USED TO DISTINGUISH THE TWO CORRESPONDING VEGETATION CLASSES

	Bottomland forest	Saline marsh	Intermediate marsh
Agriculture	(0.13, 1.98) (E, F) (0.20, 1.98) (E, N)	(0.80, 1.99) (R, N)	
Saline marsh			(0.30, 2.03) (E, F)
Freshwater marsh			(1.34, 2.09) (E, F) (1.28, 2.10) (E, N) (1.66, 2.05) (R, F)

Note: E: ERS; R: RADARSAT; N: leaf-on season; F: leaf-off season.

Among the marshes, brackish marshes are characterized by the consistently lowest σ° of RADARSAT-1. A saline marsh may be identified by its highest averaged $\sigma^\circ_{RADARSAT}$ among marsh classes. Freshwater and intermediate marshes have very similar σ°. However, the averaged $\sigma^\circ_{ERS\_LEAF\_OFF}$ for intermediate marshes is marginally higher than $\sigma^\circ_{ERS\_LEAF\_ON}$. The seasonally averaged σ° of both saline and brackish marshes behaves quite distinctively compared to that of freshwater and intermediate marshes; therefore, we may infer that this characteristic may be useful in mapping changes in salinity in coastal wetlands.

Radar Backscattering and Vegetation Index

We have shown that seasonal variation of radar backscattering signal responds to changes in structural elements of vegetation classes. The seasonal changes of vegetation cover can also be detected by optical sensors. In this section, we further investigate how the radar signal can be related to land-cover information derived from optical sensors by comparing σ° to NDVI.

We use NDVI prepared by the U.S. Geological Survey (USGS) Center for Earth Resources Observation and Science (EROS) from Advanced Very High Resolution Radiometer (AVHRR) instruments on-board National Oceanic and Atmospheric Administration (NOAA) satellites. The classes of NDVI are summarized according to 1992 National Land Cover Data (NLCD) (**http://landcover.usgs.gov/natllandcover.php**) by taking the majority composition of NLCD pixels within a 1 km^2 pixel of AVHRR imagery (J. Brown, personal communication, 2006). Healthy vegetation absorbs most of the visible light that hits it and reflects a large portion of near-infrared light, resulting in high NDVI values. Unhealthy or sparse vegetation reflects more visible light and less near-infrared light, resulting in low NDVI values.

Classes of vegetation defined by GAP and the National Wetland Research Center (NWRC) are compared with those defined by NLCD. Bottomland forest is comparable to NLCD's "deciduous forest" type, where 75 percent or more of the tree species shed foliage simultaneously in response to seasonal change. Likewise, swamp forest is comparable to NLCD's "woody wetlands" class, where forest or shrubland vegetation accounts for 25 to 100 percent of the cover, and the soil or substrate is periodically saturated or covered with water. The four types of marshes in our study area are comparable to NLCD's "emergent herbaceous wetlands," where perennial herbaceous vegetation accounts for 75 to 100 percent of the cover, and the soil or substrate is periodically saturated or covered with water. Over the time period of SAR data used for this study, multiple AVHRR sensors are used to collect data (NOAA-11, 12, 16, and 17) (J. Eidenshink, personal communication, 2006). For calibration purposes, we estimate the drift and bias in multiple-year NDVI data (1992 $\sim$ 1998 and 2002 $\sim$ 2004) (Figure 5a) as a second-order polynomial and remove those trends from the original NDVI time series (Figure 5b). The adjusted multi-year NDVI curves are averaged into a single year to determine typical leaf-on and leaf-off seasons. The peaks of averaged NDVI are found in the intervals of 23 April $\sim$ 06 May in the spring and 24 September $\sim$ 07 October in the fall; therefore, we have chosen the time window from around 01 May until about the end of September as the "leaf-on" season. The leaf-on season is meant to represent the time when leaves maintain fully developed conditions and is characterized by peaks in the NDVI curves in the spring and fall (Figure 5). We then define the rest of the year as the "leaf-off" season.

As we define the leaf-on season as the time period when leaves are fully developed, we should not expect significant changes in radar backscattering. The regressions between σ° and NDVI for all vegetation types do not show any significant correlation during leaf-on season because the dynamic range of the variation of NDVI is too narrow compared to radar backscatter changes. During leaf-off season, both bottomland and swamp forests show moderate to strong negative correlations with NDVI (Figures 6 and 7); R^2 is 0.78 $\sim$ 0.90 for RADARSAT and 0.49 $\sim$ 0.59 for ERS. The negative correlation during leaf-off season is likely associated with the attenuation of radar backscatter due to the growth of leaves, which reduces the amount of radar signal available for double-bounce and volume scattering. As a result, radar backscatter decreases with the increase of NDVI for swamp and bottomland forests. Therefore, negative correlation between NDVI and σ° is anticipated.

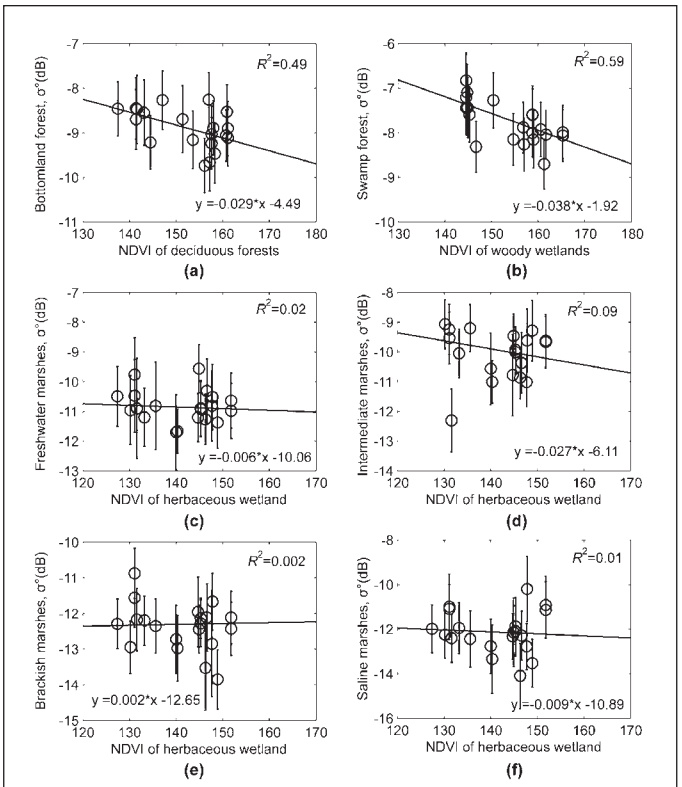

Figure 6. Regression modeling between calibrated ERS σ° and NDVI for leaf-off season.

For the marshes, $\sigma^\circ_{ERS\_LEAF\_OFF}$ does not show any correlation with NDVI. However, $\sigma^\circ_{RADARSAT\_LEAF\_OFF}$ shows impressive positive correlation with NDVI. The positive correlation implies that the radar backscattering enhances with an increase in NDVI, suggesting surface or volume scattering of the radar signal. For freshwater and intermediate marshes (R^2 = 0.78 and 0.55, respectively), positive correlation is consistent with our previous interpretation of σ°. Brackish marshes show marginally positive correlation (R^2 = 0.30); we may infer that brackish marshes are not as dense as the other marshes are to enhance σ° sufficiently with the growth of vegetation. Saline marshes show moderate positive correlation (R^2 = 0.66). This might sound contradictory to our previous interpretation. We speculate that the increase in NDVI is probably associated with the thickening of saline marsh stems, which may be translated into an increase in the double-bounced radar backscattering signal. By combining NDVI and radar backscatter signal, we can classify forests versus wetland marshes and gain additional insight into the qualitative vegetation structure. Our current results can be improved by using NDVI maps

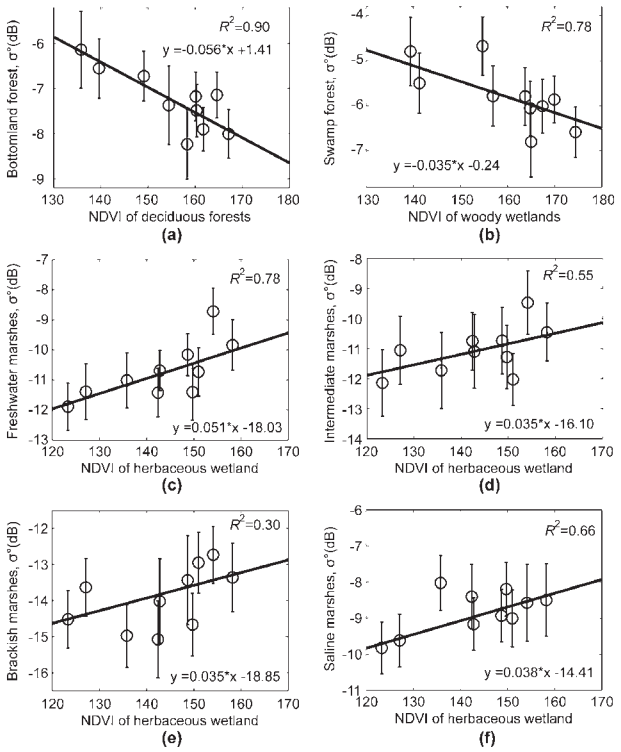

Figure 7. Regression modeling between calibrated RADARSAT-1 σ° and NDVI for leaf-off season.

derived from the higher spatial resolution imagery and more detailed classes than those by NLCD.

Conclusions

Multi-temporal RADARSAT-1 and ERS SAR images over southern Louisiana are used to study characteristics of the radar backscattering coefficient over vegetation classes. Relative radiometric calibration of the radar backscattering coefficient based on the urban backscattering coefficient is required to remove the long-term degradation of ERS-2 antenna power and scene-to-scene alternations of RADARSAT-1 antenna strength. Calibrated radar backscattering coefficients over six land-cover classes, i.e., bottomland forest, swamp forest, freshwater marsh, intermediate marsh, brackish marsh, and saline marsh are systematically analyzed to understand the relationship between seasonal variation of σ° and vegetation canopy structure. Double-bounced backscattering is the dominant scattering mechanism for swamp forest and saline marsh. Volume scattering dominates freshwater and intermediate marshes and bottomland forests. Brackish marsh is likely dominated by volume scattering and specular scattering. RADARSAT-1 backscattering coefficients offer better separability among different wetland land-cover types than ERS data, suggesting C-band HH polarization is more sensitive to structural differences than C-band VV polarization.

We demonstrate that radar backscattering coefficients during leaf-off season have strong correlations with NDVI. Swamp and bottomland forests show negative correlations between NDVI and SAR data, while marshes exhibit positive correlations with RADARSAT data only. We find that the correlation between σ° and NDVI is useful in differentiating between forests and coastal marshes and in refining our understanding of vegetation structure. Our study demonstrates that satellite SAR can be useful for coastal wetland characterization and monitoring. We anticipate that, in the future, polarimetric SAR data will significantly improve our ability for coastal wetlands classification via a physically sound model of vegetation structure.

Acknowledgments

ERS-1/ERS-2 SAR images are copyrighted © 1992, 1993, 1996, 1997, and 1998 by the European Space Agency (ESA) and were provided by the ESA using the Category-1 Project 2853. RADARSAT-1 images are copyrighted © 2002, 2003, and 2004 by the Canadian Space Agency (CSA) and were provided by the Alaska Satellite Facility (ASF). This research was supported by funding from the U.S. Geological Survey (USGS) Director Venture Capital Fund, USGS Eastern Region Venture Capital Fund, USGS Land Remote Sensing Program, and USGS contract O3CRCN0001. We thank Elijah Ramsey and Terry Sohl for careful reviews and constructive comments.

References

Baghdadi, N., M. Bernier, R. Gauthier, and I. Neeson, 2001. Evaluation of C-band SAR data for wetlands mapping, *International Journal of Remote Sensing*, 22(1):71–88.

Barras, J., S. Beville, D. Britsch, S. Hartley, S. Hawes, J. Johnston, P. Kemp, Q. Kinler, A. Martucci, J. Porthouse, D. Reed, K. Roy, S. Sapkota, and J. Suhayda, 2003. *Historical and Projected Coastal Louisiana Land Changes: 1978–2050*, USGS Open File Report 03–334:39.

Barras, J., J. Bolles, R. Carriere, D. Daigle, D. Demcheck, D. Dittmann, D. Etheridge, A. Lee, J. Morgan, L. Noble, D. Purrington, K. Radlauer, C.S. Romain, and L. Scioneaux, 2006. *Types of Wetlands*, America's Wetland Resource Center, Loyola University, New Orleans, Louisiana.

Bourgeau-Chavez, L.L., E.S. Kasischke, S.M. Brunzell, J.P. Mudd, K.B. Smith, and A.L. Frick, 2001. Analysis of space-borne SAR data for wetland mapping in Virginia riparian ecosystems, *International Journal of Remote Sensing*, 22(18):3665–3687.

Bourgeau-Chavez, L.L., K.B. Smith, S.M. Brunzell, E.S. Kasischke, E.A. Romanowicz, and C.J. Richardson, 2005. Remote monitoring of regional inundation patterns and hydroperiod in the greater Everglades using synthetic aperture radar, *Wetlands*, 25(1):176–191.

Chabreck, R.H., 1972. Vegetation, water, and soil characteristics of the Louisiana coastal region, *LSU Agriculture Experiment Station Bulletin* (664):1–72.

Costa, M.P.F., 2004. Use of SAR satellites for mapping zonation of vegetation communities in the Amazon floodplain, *International Journal of Remote Sensing*, 25(10):1817–1835.

Costa, M.P.F., O. Niemann, E. Novo, and F. Ahern, 2002. Biophysical properties and mapping of aquatic vegetation during the hydrological cycle of the Amazon floodplain using JERS-1 and RADARSAT, *International Journal of Remote Sensing*, 23(7):1401–1426.

Davis, J., 1986. *Statistics and Data Analysis in Geology*, Second edition, Wiley, New York 646 p.

Ferretti, A., C. Prati, and F. Rocca, 2001. Permanent scatterers in SAR interferometry, *IEEE Transactions on Geosciences and Remote Sensing*, 39(1):8–20.

Frost, V.S., J.A. Stiles, K.S. Shanmugan, and J.C. Holtzman, 1982. A model for radar images and its application to adaptive digital filtering of multiplicative noise, *IEEE Transactions in Pattern Analysis Machine Intelligence*, PAMI-4, pp. 157–165.

Grings, F.M., P. Ferrazzoli, J.C. Jacobo-Berlles, H. Karszenbaum, J. Tiffenberg, P. Pratolongo, and P. Kandus, 2006. Monitoring flood condition in marshes using EM models and ENVISAT ASAR observations, *IEEE Transactions on Geoscience and Remote Sensing*, 44(4):936–942.

Hess, L.L., and J.M. Melack, 1994. Mapping wetland hydrology and vegetation with synthetic aperture radar, *International Journal of Ecology and Environmental Sciences*, 20:197–205.

Hess, L.L., J.M. Melack, S. Filoso, and Y. Wang, 1995. Delineation of inundated area and vegetation along the Amazon floodplain with the SIR-C synthetic aperture radar, *IEEE Transactions on Geoscience and Remote Sensing*, 33(4):896–904.

Homer, C., C. Huang, L. Yang, B. Wylie, and M. Coan, 2004. Development of a 2001 National Land-Cover Database for the United States, *Photogrammetric Engineering & Remote Sensing*, 70(7):829–840.

Horritt, M.S., D.C. Mason, D.M. Cobby, I.J. Davenport, and P.D. Bates, 2003. Waterline mapping in flooded vegetation from airborne SAR imagery, *Remote Sensing and Environment*, 85:271–281.

IFAS, 2006. *Forest Ecosystems*, Institute of Food and Agricultural Sciences, University of Florida.

Karszenbaum, H., P. Kandus, J.M. Martinez, T. Le Toan, J. Tiffenberg, and M.G. Parmuchi, 2000. *ERS-2, RADARSAT SAR Backscattering Characteristics of the Parana River Delta Wetland, Argentina*, Special Publication SP-461.

Kasischke, E.S., and L.L. Bourgeau-Chavez, 1997. Monitoring south Florida wetlands using ERS-1 SAR imagery, *Photogrammetric Engineering & Remote Sensing*, 63(2):281–291.

Kiage, L.M., N.D. Walker, S. Balasubramanian, A. Babin, and J. Barras, 2005. Applications of RADARSAT-1 synthetic aperture radar imagery to assess hurricane-related flooding of coastal Louisiana, *International Journal of Remote Sensing*, 26(24):5359–5380.

LCWCRTF/WCRA, 1998. *Coast 2050: Toward a Sustainable Coastal Louisiana*, Louisiana Department of Natural Resources, Baton Rouge, Louisiana, p. 161.

Le Toan, T., F. Ribbes, L.-F. Wang, N. Floury, K.-H. Ding, J.A. Kong, M. Fujita, and T. Kurosu, 1997. Rice crop mapping and monitoring using ERS-1 data based on experiment and modeling results, *IEEE Transactions on Geoscience and Remote Sensing*, 35(1):41–56.

Loveland, T.L., and D.M. Shaw, 1996. Multiresolution land characterization: Building collaborative partnerships, *Proceedings of the ASPRS/GAP Symposium*, Charlotte, North Carolina, pp. 83–89.

Lu, Z., M. Crane, O. Kwoun, C. Wells, C. Swarzenski, and R. Rykhus, 2005. C-band Radar Observes Water-level Change in Swamp Forests, *EOS Transactions, AGU*, 86(14):141.

Lu, Z., and O. Kwoun, 2008. Radarsat-1 and ERS interferometric coherence analysis over southeastern coastal Louisiana: Implication for mapping water-level changes beneath swamp forests, *IEEE Transactions on Geoscience and Remote Sensing*, 46(8):2167–2184.

Lu, Z., and D. Meyer, 2002. Study of high SAR backscattering due to an increase of soil moisture over less vegetated area: Its implication for characteristic of backscattering, *International Journal of Remote Sensing*, 23(6):1065–1076.

Nelson, S.A.C., P. Soranno, and J. Qi, 2002. Land-cover change in upper Barataria Basin Estuary, Louisiana, 1972–1992: Increase in wetland area, *Environmental Management*, 29(5):716–727.

Ramsey III, E.W., 1995. Monitoring flooding in coastal wetlands by using radar imagery and ground-based measurements, *International Journal of Remote Sensing*, 16(13):2495–2502.

Ramsey III, E.W. (editor), 1998. *Radar Remote Sensing of Wetlands*, Ann Arbor Press, Inc., Ann Arbor, Michigan, pp. 211–243.

Ramsey III, E.W., 1999. Radar remote sensing of wetlands, *Remote Sensing Change Detection* (R.S. Lunetta and C.D. Elvidge, editors), Ann Arbor Press, Chelsea, Michigan, pp. 211–243.

Ramsey III, E.W., Z. Lu, A. Rangoonwala, and R. Rykhus, 2006. Multiple baseline radar interferometry applied to coastal land cover classification and change analyses, *GIScience and Remote Sensing*, 43(4):283–309.

Russell, P.R., Z. Lu, and B. Jones, 2005. Satellite imagery maps: Hurricane Katrina induced flooding and oil slicks, *EOS Transactions*, 86(41):381–382.

Sadre, A.S., A. Douglas, and W.-S. Liou, 1995. Accuracy of Landsat-TM and GIS rule-based methods for forest wetland classification in Maine, *Remote Sensing and Environment*, 53:133–144.

Simard, M., G. De Grandi, S. Saatchi, and P. Mayaux, 2002. Mapping tropical coastal vegetation using JERS-1 and ERS-1 radar data with a decision tree classifier, *International Journal of Remote Sensing*, 23(7):1461–1474.

Stehman, S.V., J.D. Wickham, J.H. Smith, and L. Yang, 2003. Thematic accuracy of the 1992 National Land-Cover Data for the eastern United States: Statistical methodology and regional results, *Remote Sensing and Environment*, 86:500–516.

Townsend, P.A., 2002. Estimating forest structure in wetlands using multitemporal SAR, *Remote Sensing and Environment*, 79:288–304.

Ulaby, F.T., and C.M. Dobson, 1989. *Handbook of Radar Scattering Statistics for Terrain*, Artech House, Inc., Norwood, Massachusetts, 357 p.

USACOE, 2004. Louisiana Coastal Area (LCA), *Louisiana Ecosystem Restoration Study*, U.S. Army Corps of Engineers-New Orleans District.

USGS-NWRC, 1998. *Land cover Classification for the Louisiana GAP Analysis Project*, USGS National Wetlands Research Center

USGS-NWRC, 2005. *2004 Digital Orthophoto Quarter Quadrangles for Louisiana*, U.S. Geological Survey, National Wetlands Research Center, Lafayette, Louisiana,

Wegmüller, U., and C. Werner, 2003. *GAMMA MSP Reference Manual*, Gamma Remote Sensing.